Applied Physics A (2018) 124:792
https://doi.org/10.1007/s00339-018-2198-9

Applied Physics A
Materials Science & Processing

Influence of post-deposition annealing on the chemical states of crystalline tantalum pentoxide films

Israel Perez[1] · Víctor Sosa[2] · Fidel Gamboa[2] · José Trinidad Elizalde Galindo[3] · José L. Enríquez-Carrejo[3] · Rurik Farías[3] · Pierre Giovanni Mani González[3]

Received: 3 October 2018 / Accepted: 16 October 2018

Abstract
We investigate the effect of post-deposition annealing (for temperatures from 848 K to 1273 K) on the chemical properties of crystalline Ta_2O_5 films grown on Si(100) substrates by radio frequency magnetron sputtering. The atomic arrangement, as determined by X-ray diffraction, is predominately hexagonal ($\delta - Ta_2O_5$) for the films exposed to heat treatments at 948 K and 1048 K; orthorhombic ($\beta - Ta_2O_5$) for samples annealed at 1148 K and 1273 K; and amorphous for samples annealed at temperatures below 948 K. X-ray photoelectron spectroscopy for Ta 4*f* and O 1*s* core levels were performed to evaluate the chemical properties of all films as a function of annealing temperature. Upon analysis, it is observed the Ta 4*f* spectrum characteristic of Ta in Ta^{5+} and the formation of Ta-oxide phases with oxidation states Ta^{1+}, Ta^{2+}, Ta^{3+}, and Ta^{4+}. The study reveals that the increase in annealing temperature increases the percentage of the state Ta^{5+} and the reduction of the others indicating that higher temperatures are more desirable to produce Ta_2O_5, however, there seems to be an optimal annealing temperature that maximizes the O% to Ta% ratio. We found that at 1273 K the ratio slightly reduces suggesting oxygen depletion.

1 Introduction

In the last years, tantalum pentoxide (Ta_2O_5) has been considered as a good candidate for technological applications such as gas detector, insulator, catalyst, and storage capacitor [1–3]. This is due to its high dielectric constant, high refractive index ($n = 2.18$ at $\lambda = 550$ nm), and a wide optical band gap of ~4.0 eV [4–7]. Ta_2O_5 crystallizes in several polymorphs depending on the synthesis methods and the temperatures in post-deposition heat treatments. For annealing temperatures below 873 K, Ta_2O_5 is amorphous, but for temperatures between 873 K and 1523 K two crystalline phases show up, namely: hexagonal (δ phase) and orthorhombic (β phase) [8–11].

The chemical, physical, and structural properties of Ta_2O_5 films deeply depend on the fabrication processes. In the last years, a great number of methods such as PLD, rf sputtering, ion-assisted deposition, and EBE have been used to grow Ta_2O_5 films [12–17]. In general, the oxygen to tantalum ratio is not stoichiometric and the chemical composition depends strongly on the methods employed. To ensure full oxygenation of the films, post-deposition annealing is carried out [18–20]. There has been evidence of crystalline phase transition from hexagonal to orthorhombic as the annealing temperature increases [21]. As a result of this, significant changes on the physical and chemical properties of the samples are expected. Despite that there is a wide number of works studying the chemical properties of amorphous Ta_2O_5 films [17, 22–25], to the best of our knowledge, there are a few works focused on studying these properties for the crystalline phases.

In this work, we investigate the annealing temperature dependence of the chemical properties in crystalline Ta_2O_5 films deposited on Si substrates by RF magnetron sputtering. For this purpose, we prepared several Ta films and

✉ Israel Perez
israel.perez@uacj.mx

[1] National Council of Science and Technology (CONACYT)-Institute of Engineering and Technology, Universidad Autónoma de Ciudad Juárez, Av. del Charro 450 Col. Romero Partido, 32310 Juárez, Chihuahua, Mexico

[2] Applied Physics Department, CINVESTAV Unidad Mérida, km 6 Ant. Carretera a Progreso, A.P. 73, 97310 Mérida, Yucatán, Mexico

[3] Institute of Engineering and Technology, Universidad Autónoma de Ciudad Juárez, Av. del Charro 450 Col. Romero Partido, 32310 Juárez, Chihuahua, Mexico

Published online: 01 November 2018

exposed them to annealing temperatures ranging from 848 K to 1273 K. Their crystalline structure was evaluated with XRD (X-ray diffraction) and the chemical properties such as atomic concentration, chemical states, and atomic bonding were studied by X-ray photoelectron spectroscopy (XPS).

2 Experimental

2.1 Film growth and annealing

Six amorphous Ta films were deposited at room temperature on Si(100) substrates by the RF magnetron sputtering technique. The deposition took place in a vacuum chamber with a base pressure of 6.6×10^{-5} mbar. Argon gas (99.9% purity) was flushed into the chamber to obtain a working pressure of $(2.6 \pm 0.1) \times 10^{-2}$ mbar. Before deposition, the substrates were cleaned up by several baths of distilled water, acetone, and ethanol. To eliminate the native oxide layer on the target, a 5 min presputtering was conducted before deposition. The deposition was carried out using a 2.5 inch Ta target with 99.95% purity and a sputtering power of 120 W; resulting in a deposition rate of 2.8 Å·s^{-1} and a thickness for all films of 2.4 μm. The target-to-substrate distance was about 12 cm and during film growth no oxygen was flushed into the chamber. To induce the desired crystalline phase, i.e., Ta_2O_5, five films were exposed to post-deposition heat treatments in air for 1 h at different annealing temperatures, namely (848, 948, 1048, 1148, 1273) K using a Thermo Scientific Thermolyne cylindrical furnace (model F21135). To associate the annealing temperature to the samples, the films were labeled F848, F948, F1048, F1148, and F1273. The remaining film, labeled F298, was kept for future reference and was not subjected to any heat treatment. Table 1 gives the annealing temperature T_{ann} and the crystalline phase of the films.

2.2 Characterization

A Siemens diffractometer model D-5000 with Cu K_{α_1} radiation ($\lambda = 1.5406$ Å) was used to evaluate the atomic structure of the samples. Steps of 0.02° with a time per step of 3 s and operating parameters of 34 kV and 25 μA were used to obtain the XRD patterns. A Thermo Scientific K-Alpha XPS spectrometer with an Al K_α X-ray source set to 12 kV and 40 W was used to analyze the chemical properties of the films. For the XPS surveys and scans, we used steps of 1 eV and 0.1 eV, respectively; the beam spot had a diameter of 400 μm and made an angle relative to the sample of 30°. Chemical properties were assessed measuring the Ta 4*f* and O 1*s* core levels. The atomic composition, chemical states, and atomic bonding were determined by deconvolution of the Ta 4*f* and O 1*s* spectra using Shirley-Sherwood background and Voigt functions [Gaussian $\sigma = (1.43, 0.9)$ eV and Lorentzian $\gamma = 0.02$ eV] as implemented in the AAnalizer software [26].

Table 1 Annealing temperature T_{ann} and determined crystalline phase for the films

Film	$\frac{T_{\text{ann}}}{K}$	Phase
F298	298	Amorphous
F848	848	Amorphous
F948	948	δ
F1048	1048	δ
F1148	1148	β
F1273	1273	β

3 Results and discussion

3.1 Crystalline structure

To evaluate the crystalline structure of our samples, we performed XRD measurements. Samples F298 and F848 showed no diffraction patterns, indicating a disordered atomic structure (see Fig. 1). The rest of the samples exhibit a crystalline structure. For the sake of phase indexation, we compared our measurements with several references from the Powder Diffraction File (PDF) dababase under the

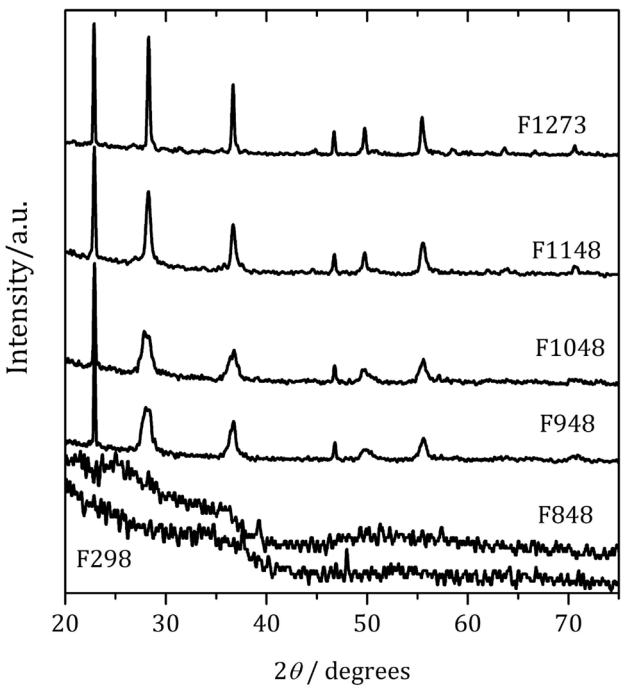

Fig. 1 X-ray diffraction patterns for the crystalline films. The patterns for the samples F948 and F1048 are indexed to the δ phase and the patterns for F1148 and F1273 are indexed to the β phase of Ta_2O_5. Samples F298 and F848 are amorphous

International Centre for Diffraction Data (ICDD) implemented in the software of the diffractometer. From a list of at least six PDFs (even among these references we spotted slight discrepancies), the films F948 and F1048 can be indexed to the hexagonal phase $\delta - Ta_2O_5$ with PDF 00-019-1299; lattice parameters $a = b = 3.6240$ Å, $c = 3.8800$ Å, $\alpha = \beta = 90°$, and $\gamma = 120°$; spatial group $P6\,/\,mmm$ [27, 28], whereas the films F1148 and F1273 can be indexed to the orthorhombic phase $\beta - Ta_2O_5$ with either PDF 00-025-0922; lattice parameters $a = 6.1980$ Å, $b = 40.2900$ Å, $c = 3.8880$ Å, and $\alpha = \beta = \gamma = 90°$; spatial group $P2_12_12$; or PDF 01-089-2843; lattice parameters $a = 6.2000$ Å, $b = 3.6600$ Å, $c = 3.8900$ Å, and $\alpha = \beta = \gamma = 90°$; spatial group $Amm2$. In Table 1, the phases for all films are summarized. Figure 2 shows the best matches, there we can see that the pattern of F1273 shows a much richer pattern than the pattern due to F948. It is evident that F1273 exhibits a series of small reflections along the whole pattern that match the reference pattern PDF 025-0922. It is important to underline that so far there has not been a consensus regarding the spatial symmetry of these two phases, and, due to the overlapping of several peaks, one cannot rule out the coexistence of both phases [21, 29–36]. To the best of our knowledge, at least 12 spatial groups has been proposed and we do think it is not worth computing the lattice parameters or conducting a Rietveld refinement, since these depend on the particular choice of the group symmetry. The precise determination of both the crystalline structure and the spatial symmetry are beyond the scope of the present investigation.

The crystallite size D was estimated using the so-called Scherrer relation

$$D = \frac{K\lambda}{\Gamma \cos\theta}, \tag{1}$$

where we used $K = 0.9$, $\lambda = 1.5406$ Å and Γ is the full width at half maximum. For our calculations, we used the peak at $2\theta = 28.3°$ and found that Γ =(0.79, 0.69, 0.52, 0.27)°. With these values, we found the size to be D =(10, 12, 16, 30) nm, respectively.

It is worth mentioning that Ta_2O_5 is the most stable oxide of Ta; other oxides such as TaO, Ta_2O, TaO_2, Ta_2O_3 are difficult to synthesize as pure phases (except for TaO_x) and usually appear as contamination [10]. Furthermore, most suboxides are crystalline, except for Ta_2O_3 and TaO_x that are amorphous. This issue will become important for our forthcoming discussion.

3.2 Chemical properties

The chemical properties of our samples were studied by XPS analysis. The binding energy of all spectra for Ta 4*f* and O 1*s* core levels was calibrated at 532 eV using as reference the oxygen peak. During the analysis, we also spotted traces of carbon contamination in all films as revealed by the surveys in Fig. 3.

The results of the spectra for the Ta 4*f* core level are shown in Fig. 4a. All spectra exhibit the typical spin-orbit doublet corresponding to the levels $4f_{7/2}$ and $4f_{5/2}$ located at 27.8 eV and 29.6 eV with peak splitting of 1.9 eV. The binding energies and peak splitting are characteristic of Ta^{5+} in stoichiometric amorphous Ta_2O_5 films [37–40]. A closer look at the black spectrum for the as-deposited film (F298) reveals a satellite on the low energy region. This feature

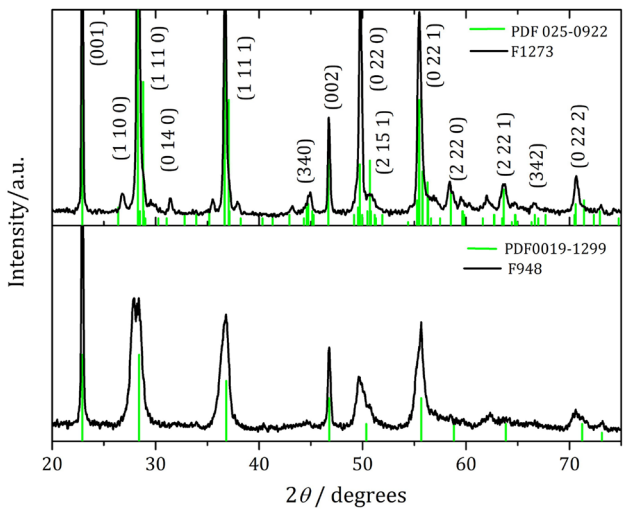

Fig. 2 Phase indexation of our samples. Samples F1148 and F1273 can be indexed to PDF 025-0922 whereas films F948 and F1048 can be indexed to PDF 0019-1299

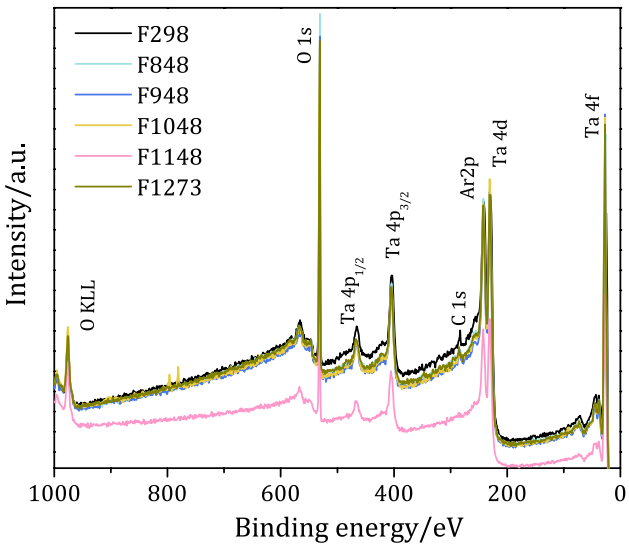

Fig. 3 XPS surveys for all samples. Some degree of carbon contamination in all samples is observed

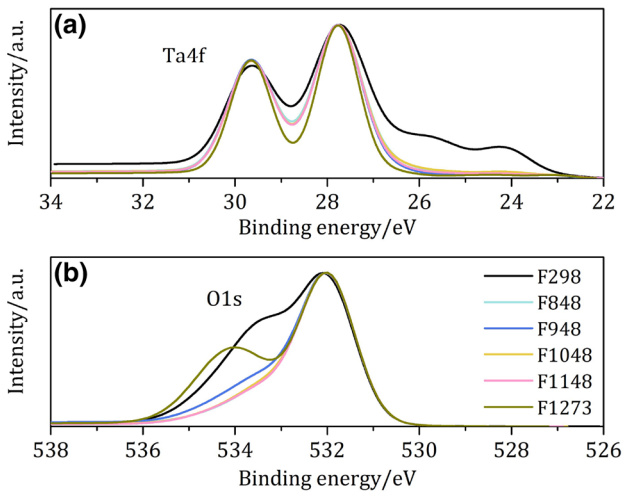

Fig. 4 Ta 4*f* (**a**) and O 1*s* (**b**) core levels for the six films

has been reported to be caused by screening of 5*d* electrons in *a*-TaO_x ($x = 1.86, 2.00$), thus suggesting the presence of Ta suboxides such as TaO_x [23]. Since this film was not exposed to a heat treatment, one would expect, besides amorphous Ta_2O_5, the appearance of other Ta suboxides that were mainly generated during deposition as there still exists residual oxygen in the deposition chamber.

As the annealing temperature is increased, the shoulder vanishes indicating that the amount of suboxides is reduced.

The O 1*s* core level gives additional information on the chemical states of our samples; the corresponding spectra are shown in Fig. 4b. We first observe a peak at 532 eV associated to Ta–O bond [39, 41]. At ~534 eV, there is a satellite whose intensity reduces as T_{ann} decreases. This feature is attributed to residual oxygen and surface contamination, mainly carbon compounds (see below). We also notice that for the sample F1273, the shoulder reappears. To verify the source of this shoulder, we sputtered the sample for 9 min with an argon ion beam with a voltage of 3 kV, and an electric current of 10 μA—the incidence angle between the sample and the ion gun was 90°. Then, the O 1*s* core level was measured and the shoulder considerably diminished (as seen in the inset of the corresponding film in Fig. 5). We thus believed that this feature is caused by contamination.

The deconvolution analysis performed on the Ta 4*f* spectra reveals that there are five contributions from five Ta oxidation states (see left column in Fig. 5). The five doublets are located, with respect to Ta $4f_{7/2}$, at binding energies of (23.0, 24.1, 25.4, 26.7, 27.8) eV with spin-orbit splittings of 1.9 eV. These binding energies are attributed to Ta^{1+}, Ta^{2+}, Ta^{3+}, Ta^{4+}, and Ta^{5+} states, respectively [22, 44, 45]. These results strongly suggest the formation of metastable phases of Ta oxides such as TaO, Ta_2O, TaO_2, TaO_x, and Ta_2O_3. However, since the XRD show no traces of crystalline phases of Ta suboxides we believe that, due to the unstable nature of these phases, during annealing the surface atoms readsorbed O to form Ta_2O_5 and the other phases are trapped in a few topmost layers [42]. On the other hand, the deconvolution of the O 1*s* spectra is shown on the right column of the same figure. There we can see that the oxygen spectrum is well-fitted with three peaks. The low energy peak is attributed to Ta–O bonding, the peak at 533 eV is due to residual oxygen and the peak at 534 eV is due to carbon contamination, most probably carbon dioxide which is quite ubiquitous in all samples [22, 23, 43]. As discussed above, the sample F1273 exhibits a pronounced satellite whose intensity was reduced after sputtering the sample for 9 min. The deconvolution confirms that this satellite is due to contamination.

To assess the effect of the annealing temperature on the chemical properties, we used the doublets of the Ta 4*f* spectra to compute the percentage of oxidation state as function of T_{ann}. Figure 6a shows the results. We can observe a monotonic increase of the percentage of Ta in the state Ta^{5+} as function of annealing temperature. The increase for the state Ta^{5+} goes from 67 to 93%, whereas the rest of the states remain below 10%. This tendency clearly demonstrates that the crystalline phases of Ta_2O_5 are favored at high temperatures. We also computed the oxygen to tantalum ratio as a function of T_{ann}. The results are given in Fig. 6b. As expected, the film F298 exhibits an O to Ta% ratio close to 1; nevertheless as the temperature is increased from 298 to 1148 K, the ratio remains around 1.5 (non-stoichiometric) and decreases to 1.2 at 1273 K. This behavior suggests that there is a range of temperature that favors the generation of tantalum pentoxide with the highest oxygen content. Accordingly, however, from 1148 to 1273 K the oxygen seems to deplete.

4 Conclusions

The atomic structure of Ta_2O_5 films was studied by X-ray diffraction. We found evidence for the presence of the hexagonal phase of Ta_2O_5 for samples annealed below 1048 K and the orthorhombic phase of Ta_2O_5 for samples annealed above 1048 K. In all these cases, there are no traces of crystalline Ta suboxides. The films exposed to heat treatments below 848 K showed no diffraction patterns and were found to be amorphous.

XPS studies were realized to characterize the chemical properties of the films. According to the analysis carried out on the spectra for Ta 4*f* and O 1*s* core levels, it can be

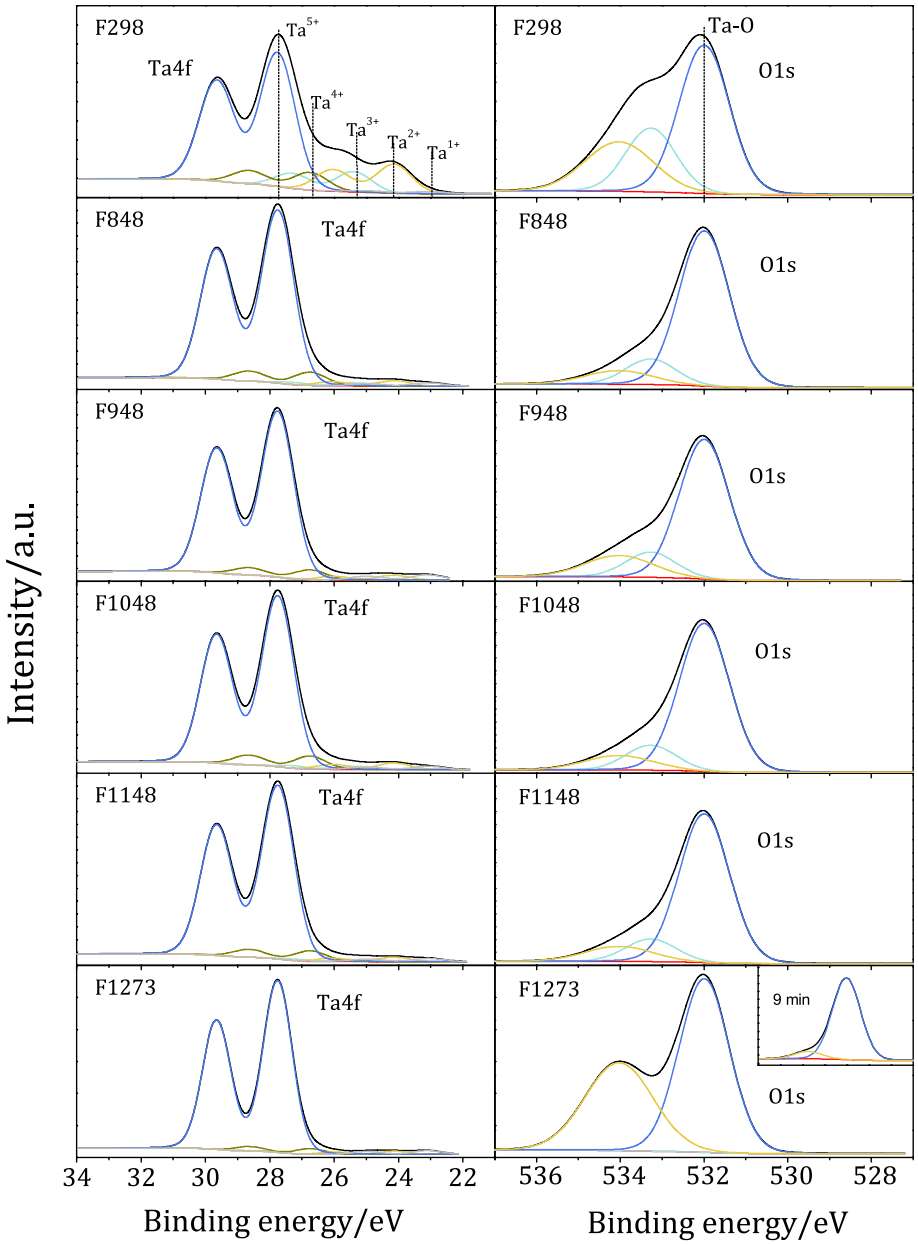

Fig. 5 Deconvolution of the Ta 4*f* (left column) and O 1*s* (right column) core levels for the six films. The inset in the O 1*s* spectrum of F1273 shows the O 1*s* spectrum after 9 min of sputtering. One can see that the satellite almost disappears and it is therefore caused by contamination

concluded that Ta suboxides show up in small amounts as revealed by the appearance of satellites in both the Ta 4*f* and O 1*s* core levels. The deconvolution of the XPS spectra strongly indicates the existence of several chemical states such as Ta^{1+}, Ta^{2+}, Ta^{3+}, Ta^{4+}, and Ta^{5+}. We conclude that as the annealing temperature is increased, the presence of the state Ta^{5+} increases, indicating that high annealing temperatures are desired to favor the generation of tantalum pentoxide. However, there seems to be a limit in the value of the annealing temperature if one wishes to avoid oxygen depletion. This is deduced by observing a reduction in the oxygen to tantalum ratio for the sample F1273.

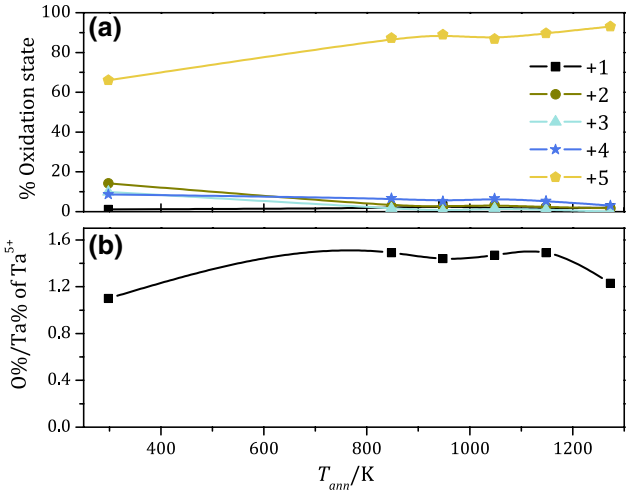

Fig. 6 Annealing temperature dependence of the oxidation state (**a**) and of the oxygen to tantalum ratio (**b**)

Acknowledgements We are grateful to Wilian Cauich and Daniel Aguilar for their technical support during the XPS and XRD sessions. Dr. Israel Perez is indebted to Dr. Alberto Herrera for helpful discussions and technical support in the XPS analysis. We also thank the anonymous reviewer and one of the editors of this journal for their comments that greatly improved the quality of this work. The authors gratefully acknowledge the support from the National Council of Science and Technology (CONACYT) Mexico and the program Cátedras CONACYT through Project 3035.

Compliance with ethical standards

Conflict of interest The authors declare no conflict of interest.

References

1. T. Kaga, H. Shinriki, F. Murai, Y. Kawamoto, Y. Nakagone, F. Takeda, K. Itoh, DRAM manufacturing in the '90s -Part 3: a case study. Semicond. Int. **6**, 98–101 (1991)
2. K.W. Kwon, C.S. Kang, S.O. Park, H.K. Kang, S.T. Ann, Thermally robust Ta_2O_5 capacitor for the 256-Mbit DRAM. IEEE Trans. Electron. Devices. **43**, 919–923 (1996)
3. C. Chaneliere, J.L. Autran, R.A.B. Devine, B. Baland, Tantalum pentoxide (Ta_2O_5) thin films for advanced dielectric applications. Mater. Sci. Eng. R-rep **22**, 269–322 (1998)
4. C. Chaneliere, S. Four, J.L. Autran, R.A.B. Devine, N.P. Sandler, Properties of amorphous and crystalline Ta_2O_5 thin films deposited on Si from a $Ta(OC_2H_5)_5$ precursor. Electrochem. J. Appl. Phys. **83**, 4823–4829 (1998)
5. R.H. Dennard, F.H. Gaensslen, H. Yu, V.L. Rideout, E. Bassous, A.R. LeBlanc, Design of ion-implanted MOSFET's with very small physical dimensions. IEEE J. Solid-State Circ. **9**, 256–268 (1974)
6. S. Shibata, Dielectric constants of Ta_2O_5 thin films deposited by r.f. sputtering. Thin Solid Films **277**, 1–4 (1996)
7. E. Atanassova, Thin RF sputtered and thermal Ta_2O_5 on Si for high density DRAM application. Microelectron. Reliab. **39**, 1185–1217 (1999)
8. J.D.T. Kruschwitz, W.T. Pawlewicz, Optical and durability properties of infrared transmitting thin films. Appl. Opt. **36**, 2157–2159 (1997)
9. C. Chaneliere, S. Foura, J.L. Autran, R.A.B. Devine, Comparison between the properties of amorphous and crystalline Ta_2O_5 thin films deposited on Si. Microelectron. Reliab. **39**, 261–268 (1999)
10. S.P. Garg, N. Krishnamurthy, A. Awashi, M. Venkatraman, The O-Ta (Oxygen-Tantalum) system. J. Phase Equilib. **17**, 63–77 (1996)
11. K.T. Jacob, C. Shekhar, Y. Waseda, An update on the thermodynamics of Ta_2O_5. J. Chem. Thermodyn. **41**, 748–753 (2009)
12. E. Atanassova, T. Dimitrova, J. Koprinarova, AES and XPS study of thin RF-sputtered Ta_2O_5 layers. Appl. Surf. Sci. **84**, 193–202 (1995)
13. H. Shinriki, M. Nakata, UV-O_3 and Dry-O_2: Two-step Annealed Chemical Vapor-Deposited Ta_2O_5 Films for Storage Dielectrics of 64-Mb DRAMs. IEEE Trans. Electron Devices ED. **38**, 455–462 (1991)
14. S. Kamiyama, P.-Y. Lesaicherre, H. Suzuki, A. Sakai, I. Nishiyama, A. Ishitani, J. Electrochem. Soc. **140**, 1617 (1993)
15. G.Q. Lo, D.L. Kwong, S. Lee, Appl. Phys. Lett. **62**, 973 (1993)
16. Y. Kuo, Reactive Ion Etching of Sputtered Deposited Tantalum Oxide and its Etch Selectivity to Tantalum. J. Electrochem. Soc. **139**, 579–583 (1992)
17. N. Donkov, A. Zykova, V. Safonov, R. Rogowska, J. Smolik, Tantalum pentoxide ceramic coatings deposition on ti4a16v substrates for biomedical applications. Probl. At. Sci. Technol. Plasma Phys. Ser. **17**, 131–133 (2011)
18. T. Dimitrova, U,K. Arshak, E. Atanassova, Crystallization effects in oxygen annealed Ta_2O_5 thin films on Si. Thin Solid Films **38**, 31–38 (2001)
19. S.-J.J. Wu, B. Houng, B.S. Huang, Effect of growth and annealing temperatures on crystallization of tantalum pentoxide thin film prepared by RF magnetron sputtering method. J. Alloys Compd. **475**, 488–493 (2009)
20. D. Cristea, D. Constantin, A. Crisan, C.S. Abreu, J.R. Gomes, N.P. Barradas, E. Alves, C. Moura, F. Vaz, L. Cunha, Properties of tantalum oxynitride thin films produced by magnetron sputtering: the influence of processing parameters. Vacuum **98**, 63–69 (2013)
21. I. Perez, J.L. Enríquez-Carrejo, V. Sosa, F. Gamboa, J.R. Farias-Mancillas, J.T. Elizalde-Galindo, Evidence for structural transition in crystalline tantalum pentoxide films grown by RF magnetron sputtering. J. Alloys. Comp. **712**, 303–210 (2014)
22. E. Atanassova, D. Spassov, X-ray photoelectron spectroscopy of thermal thin Ta_2O_5 films on Si. Appl. Surf. Sci. **135**, 71–82 (1998)
23. Takashi Tsuchiya, Hideto Imai, Shogo Miyoshi, Per-Anders Glans, Jinghua Guo, Shu Yamaguchi, X-ray absorption, photoemission spectroscopy, and Raman scattering analysis of amorphous tantalum oxide with a large extent of oxygen nonstoichiometry. Phys. Chem. Chem. Phys. **13**, 17013–17018 (2011)
24. S.-C. Wang, K.-Y. Liu, J.-L. Huang, Tantalum oxide film prepared by reactive magnetron sputtering deposition for all-solid-state electrochromic device. Thin Solid Films **520**, 1454–1459 (2011)
25. S.V. Jagadeesh-Chandra, C.-J. Choi, S. Uthanna, G. Mohan-Rao, Structural and electrical properties of radio frequency magnetron sputtered tantalum oxide films: Influence of post-deposition annealing. Mater. Sci. Semicond. Process. **13**, 245–251 (2010)
26. A. Herrera-Gomez, M. Bravo-Sanchez, O. Ceballos-Sanchez, M.O. Vazquez-Lepe, Practical Methods for Background Subtraction in Photoemission Spectra. Surf. Interface Anal. **46**, 897–905 (2014)
27. A. Fukumoto, K. Miwa, Prediction of hexagonal Ta_2O_5 structure by first-principles calculations. Phys. Rev. B **55**, 11155 (1997)

28. Y.-N. Wu, L. Li, H.-P. Cheng, First-principles studies of Ta_2O_5 polymorphs. Phys. Rev. B **83**, 144105 (2011)
29. S. Pérez-Walton, C. Valencia-Balvín, A.C.M. Padilha, G.M. Dalpian, J.M. Osorio-Guillén, A search for the ground state structure and the phase stability of tantalum pentoxide. J. Phys. Condens. Matt. **28**, 035801–11 (2016)
30. J.Y. Kim, B. Magyari-Köpe, K.-J. Lee, H.-S. Kim, S.-H. Lee, Y. Nishi, Electronic structure and stability of low symmetry Ta_2O_5 polymorphs. Phys. Status Solidi RRL **8**, 560–565 (2014)
31. S.-H. Lee, J. Kim, S.-J. Kim, S. Kim, G.-S. Park, Hidden structural order in orthorhombic Ta_2O_5. Phys. Rev. Lett. **110**, 235502–5 (2013)
32. J. Lee, W. Lu, E. Kioupakis, Electronic properties of tantalum pentoxide polymorphs from first-principles calculations. Appl. Phys. Lett. **105**, 202108–5 (2014)
33. Z. Helali, M. Calatayud, C. Minot, Novel Delta-Ta_2O_5 Structure Obtained from DFT Calculations. J. Phys. Chem. C. **118**, 13652–13658 (2014)
34. Y. Guo, J. Robertson, Comparison of oxygen vacancy defects in crystalline and amorphous Ta_2O_5. Microelectron. Eng. **147**, 254–259 (2015)
35. J.-Y. Kim, B. Magyari-Köpe, Y. Nishi, J.-H. Ahn, First-principles study of carbon impurity effects in the pseudo-hexagonal Ta_2O_5. Curr. Appl. Phys. **16**, 638–643 (2016)
36. Y. Yang, Y. Kawazoe, Prediction of a new ground-state crystal structure of Ta_2O_5. Phys. Rev. Mat. **2**, 034602 (2018)
37. X.M. Wu, P.K. Wu, T.M. Lu, E.J. Rymaszewski, Reactive sputtering deposition of low temperature tantalum suboxide thin films. Appl. Phys. Lett. **62**, 3264–3266 (1993)
38. K. Chen, G.R. Yang, M. Nielsen, T.M. Lu, E.J. Rymaszewski, X-ray photoelectron spectroscopy study of Al/Ta_2O_5 and Ta_2O_5/Al buried interfaces. Appl. Phys. Lett. **70**, 399–401 (1997)
39. A. Muto, F. Yano, Y. Sugawara, S. Iijima, The study of ultrathin tantalum oxide films before and after annealing with X-ray photoelectron spectroscopy. Jpn. J. Appl. Phys. **33**, 2699–2702 (1994)
40. R. Simpson, R.G. White, J.F. Watts, M.A. Baker, XPS investigation of monatomic and cluster argon ion sputtering of tantalum pentoxide. Appl. Surf. Sci. **405**, 79–87 (2017)
41. H. Szymanowski, O. Zabeida, J.E. Klemberg-Sapieha, L. Martinu, Optical properties and microstructure of plasma deposited Ta_2O_5 and Nb_2O_5 films. J. Vac. Sci. Technol. A **23**, 241–247 (2005)
42. E. Atanassova, M. Kalitzova, G. Zollo, A. Paskaleva, A. Peeva, M. Georgieva, G. Vitalib, High temperature-induced crystallization in tantalum pentoxide layers and its influence on the electrical properties. Thin Solid Films **426**, 191–199 (2003)
43. O. Kerrec, D. Devilliers, H. Groult, P. Marcus, Study of dry and electrogenerated Ta_2O_5 and Ta/Ta_2O_5/Pt structures by XPS. Mat. Sci. Eng **B55**, 134–142 (1998)
44. M.V. Ivanov, T.V. Perevalov, V.S. Aliev, V.A. Gritsenko, V.V. Kaichev, Electronic structure of Ta_2O_5 with oxygen vacancy: ab initio calculations and comparison with experiment. J. Appl. Phys. **110**, 024115 (2011)
45. M.V. Ivanov, T.V. Perevalov, VSh Aliev, V.A. Gritsenko, V.V. Kaichev, Ab initio simulation of the electronic structure of Ta_2O_5 with oxygen vacancy and comparison with experiment. J. Exp. Theo. Phys. **112**, 1035–1041 (2011)